Cell Reports

ATR Signaling Uncouples the Role of RAD51 Paralogs in Homologous Recombination and Replication Stress Response

Graphical Abstract

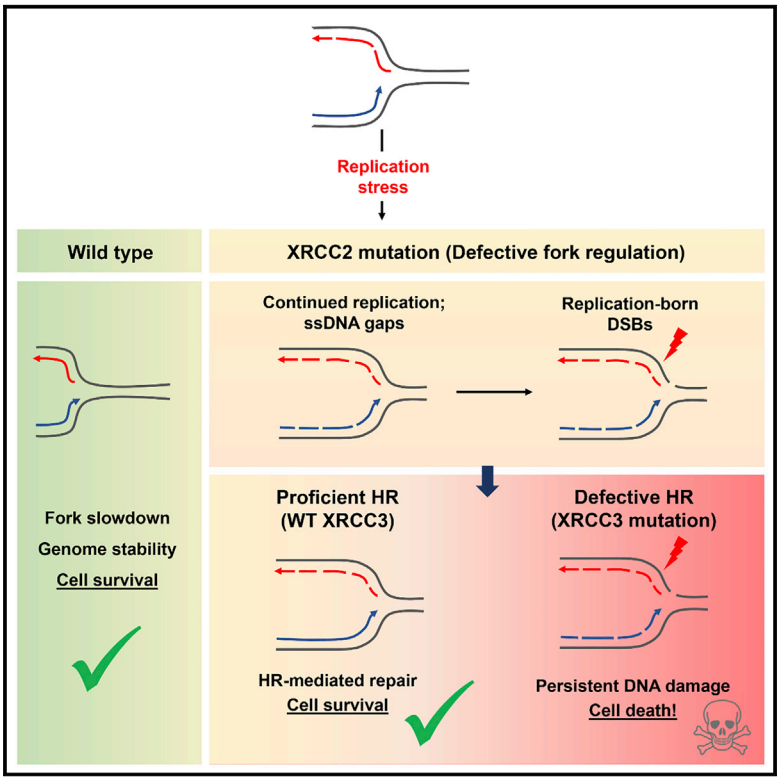

Highlights

- ATR differentially regulates RAD51 paralog complexes through XRCC2 and XRCC3
- XRCC2 S247 phosphorylation limits DNA damage during perturbed replication
- XRCC2 phospho mutant cells exhibit early XRCC3 activation during replication stress
- XRCC3-mediated repair by HR promotes survival of XRCC2 phospho mutant cells

Authors

Sneha Saxena, Suruchi Dixit, Kumar Somyajit, Ganesh Nagaraju

Correspondence

kr.somyajit@cpr.ku.dk (K.S.), nganesh@iisc.ac.in (G.N.)

In Brief

Mammalian RAD51 paralogs are conserved proteins that function in multiple aspects of genome maintenance. Here, Saxena et al. identify an ATR signaling governed pathway, wherein distinct RAD51 paralogs complexes cooperatively participate to facilitate genome integrity and cell survival during replication stress.

Saxena et al., 2019, Cell Reports *29*, 551–559
October 15, 2019 © 2019 The Author(s).
https://doi.org/10.1016/j.celrep.2019.09.008

CellPress

Cell Reports
Report

OPEN ACCESS
CellPress

ATR Signaling Uncouples the Role of RAD51 Paralogs in Homologous Recombination and Replication Stress Response

Sneha Saxena,[1] Suruchi Dixit,[1] Kumar Somyajit,[1,2,*] and Ganesh Nagaraju[1,3,*]
[1]Department of Biochemistry, Indian Institute of Science, Bangalore-560012, India
[2]Present address: Chromosome Stability and Dynamics Group, Novo Nordisk Foundation Center for Protein Research, Faculty of Health and Medical Sciences, University of Copenhagen, Blegdamsvej 3B, 2200 Copenhagen, Denmark
[3]Lead Contact
*Correspondence: kr.somyajit@cpr.ku.dk (K.S.), nganesh@iisc.ac.in (G.N.)
https://doi.org/10.1016/j.celrep.2019.09.008

SUMMARY

ATR kinase-mediated replication checkpoint is vital for genome maintenance following replication stress. Previously, we showed that XRCC2-RAD51D (DX2) sub-complex of RAD51 paralogs restrains active DNA synthesis during dNTP alterations, in a manner dependent on ATR-mediated phosphorylation of XRCC2. Here, we find that unrestrained fork progression in XRCC2 deficiency and phosphorylation defect causes replication-associated errors, subsequently resulting in genome-wide double-strand breaks (DSBs) and early activation of ATM signaling. Cells defective in XRCC2 phosphorylation exhibit ATM/ATR-mediated early activation of XRCC3 during perturbed replication, which facilitates recombination-mediated repair of the post-replicative DNA damage and thereby promotes cell viability. Collectively, our findings identify collaborative roles of RAD51 paralog complexes during replication stress and reveal their differential regulation by ATR signaling to promote cell survival and genome integrity.

INTRODUCTION

During DNA replication, various types of impediments cause slowing or stalling of the replication forks, leading to replication stress, which is a major driver of tumor progression (Técher et al., 2017; Zeman and Cimprich, 2014). Cells have hence evolved with multiple layers of regulation to manage replication stress, thereby protecting their genome against mutations and tumorigenesis (Saxena et al., 2018; Somyajit et al., 2017; Toledo et al., 2017). One of the primary functions of replication stress response is the protection of newly synthesized DNA against its nucleolytic erosion at stalled replication forks (Rickman and Smogorzewska, 2019). Fork protection involves BRCA1/2 and numerous other homologous recombination (HR) factors including RAD51, Fanconi anemia proteins, and RAD51 paralogs (Quinet et al., 2017b; Schlacher et al., 2011, 2012; Somyajit et al., 2015), in the absence of which replication forks are extensively remodeled or converted into DNA double-strand breaks (DSBs), resulting in genome instability (Liao et al., 2018).

Mammalian RAD51 paralogs are a family of conserved proteins (RAD51B, RAD51C, RAD51D, XRCC2, and XRCC3) that are involved in HR (Somyajit et al., 2010; Suwaki et al., 2011), DNA damage signaling (Badie et al., 2009; Somyajit et al., 2012, 2013), protection and restart of stalled replication forks (Somyajit et al., 2015), and mitochondrial genome stability (Mishra et al., 2018). RAD51 paralogs exist in two functionally distinct complexes (BCDX2 and CX3) (Masson et al., 2001; Wiese et al., 2002). Moreover, a RAD51 paralog sub-complex (DX2) was recently found to be involved in aligning the rate of fork progression with cellular dNTP pool alterations. Notably, this function was regulated through ATR-mediated phosphorylation of XRCC2, thus implicating the paralogs as key components of the replication stress response (Saxena et al., 2018). Interestingly, another RAD51 paralog, XRCC3, was also identified as a target of ATR kinase, but specifically in response to DSBs (Somyajit et al., 2013). Although the activation and cellular functions of these phosphorylation events have been deciphered in the context of individual complexes, whether these two signaling pathways functionally interact remains elusive.

Here, we show that ATR signaling differentially regulates two RAD51 paralog complexes (DX2 and CX3) through the phosphorylation of XRCC2 and XRCC3. We find that XRCC2 phosphorylation is specifically induced by replication stress and is crucial to prevent the generation of post-replicative gaps and genome-wide DSBs. Notably, cells defective in XRCC2 phosphorylation undergo early activation of XRCC3 during replication stress, which allows HR-mediated repair of the accumulated DNA damage and cell survival. Taken together, our findings reveal an ATR signaling governed functional interplay between RAD51 paralogs, where distinct paralog complexes appear to collaboratively facilitate genome integrity during replication stress.

RESULTS

Unrestrained DNA Replication in XRCC2 Phospho-Defective Cells Induces Post-Replicative ssDNA Gaps

XRCC2-RAD51D (DX2) complex of RAD51 paralogs was recently shown to be involved in restraining active fork

This is an open access article under the CC BY license (http://creativecommons.org/licenses/by/4.0/).

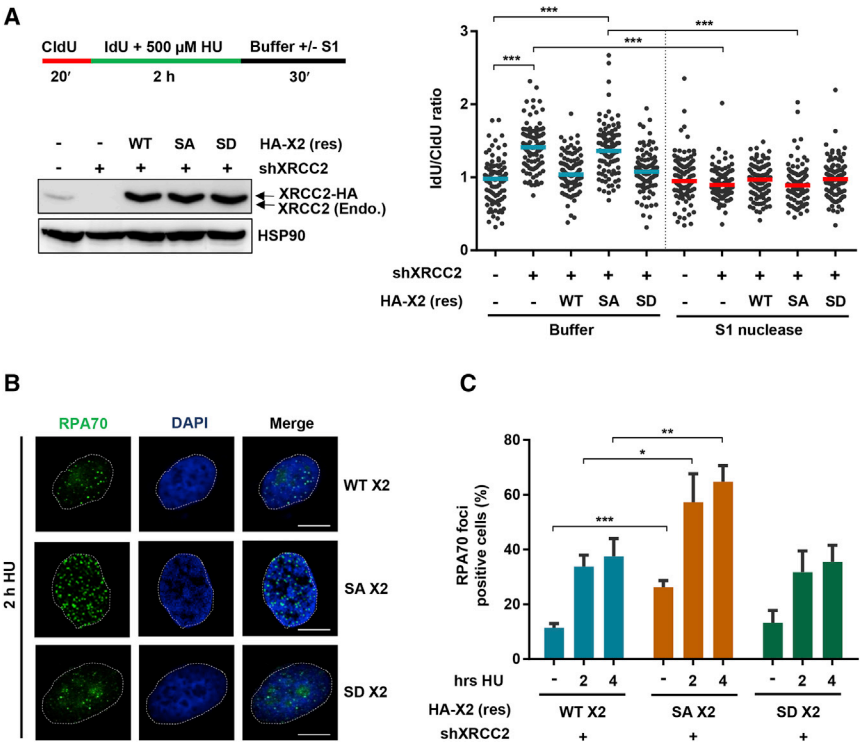

Figure 1. XRCC2 Prevents the Formation of Single-Stranded DNA (ssDNA) Gaps during Replication Stress

(A) Left: schematic of the protocol to detect ssDNA gaps using S1 nuclease. Western blot shows depletion of endogenous XRCC2 and expression of shRNA-resistant XRCC2 variants in U2OS cells. Right: IdU-to-CldU ratios in the indicated U2OS cells treated with HU, followed by incubation with buffer or S1 nuclease.

(B) Representative images of indicated U2OS cells stained for RPA70. Cells were treated with 2 mM HU for indicated times prior to pre-extraction, fixation, and immunofluorescence staining.

(C) Quantification of RPA70-positive cells under conditions as in (B). Cells with more than 20 foci were considered positive. Data are presented as mean ± SD.

Student's t test, *p < 0.05, **p < 0.01, and ***p < 0.001; n.s., non-significant. All scale bars: 10 μm. HA-X2 (res), shRNA-resistant HA-tagged XRCC2.

progression during nucleotide pool alterations. Cells deficient in XRCC2 exhibit permissive DNA replication upon dNTP perturbations, which is associated with an increase in chromosomal instability (Saxena et al., 2018). However, the mechanisms underlying this genome instability remain obscure. Recent evidence suggests that unrestrained replication during stressful conditions is associated with the formation of single-stranded DNA (ssDNA) gaps in the post-replicative genome (Lossaint et al., 2013; Peng et al., 2018). To test this possibility in XRCC2 deficient cells, we directly evaluated the presence of ssDNA gaps in ongoing forks, using a modified DNA fiber protocol (Quinet et al., 2016, 2017a). We subjected U2OS cells to 5-chloro-2′-deoxyuridine (CldU) labeling followed by a pulse of 5-iodo-2′-deoxyuridine (IdU) in the presence of the dNTP-depleting agent hydroxyurea (HU). Before spreading onto the glass slide, we permeabilized the cells and treated the nuclei with the ssDNA-specific enzyme S1 nuclease (Figure 1A). In the presence of gaps, S1 nuclease nicks the ssDNA opposite to the gap, thus converting the ssDNA gap into a DSB and resulting in shorter IdU tracts. Consistent with our previous study (Saxena et al., 2018), in the absence of S1 nuclease, XRCC2-depleted cells exhibited HU-resistant DNA synthesis, as assessed by a higher IdU/CldU ratio than control cells (Figure 1A). However, upon treatment with S1 nuclease, XRCC2-depleted cells, but not control cells, presented a significant decline in the IdU/CldU ratio (Figure 1A), suggesting the presence of ssDNA gaps in these cells. Notably, the formation of these gaps could be fully rescued by complementation with short hairpin RNA (shRNA)-resistant wild-type (WT) XRCC2, but not with the phospho-defective mutant (S247A XRCC2) (Figure 1A), suggesting a role of ATR-mediated phosphorylation of XRCC2 in preventing ssDNA generation. To confirm this, we performed ssDNA detection by native BrdU immunofluorescence assay, which revealed that levels of ssDNA were significantly elevated in XRCC2 S247A cells compared with cells expressing WT or phospho-mimetic (S247D) XRCC2 (Figure S1A). Because ssDNA is rapidly coated by the RPA heterotrimer (Maréchal and Zou, 2015), we next used RPA staining as a marker to determine the global levels of ssDNA present in cells following HU exposure. Our immunofluorescence studies showed that while HU caused a modest increase in the RPA70-positive population in WT or S247D XRCC2 cells, S247A mutants exhibited a dramatic increase in the percentage of RPA70-positive cells (Figures 1B and 1C). This was not an indirect consequence of cell cycle perturbations, as no significant difference was observed in the cell cycle profiles of these cells (Figure S1B). Together, these results indicate that XRCC2 plays a vital role in preventing ssDNA gap generation at stressed replication forks, in a manner dependent on its phosphorylation by ATR kinase.

XRCC2 Phosphorylation Prevents Replication-Born Lesions and Maintains Genome Stability following Replication Stress

ssDNA gaps within replicated DNA molecules can serve as entry points for nucleases that degrade nascent DNA during prolonged stress (Hashimoto et al., 2010). To determine whether unrestrained fork progression and subsequent ssDNA gap generation in XRCC2 deficiency results in fork degradation, we measured the ratio of IdU to CldU tract lengths following prolonged HU treatment. Indeed, XRCC2-depleted cells and cells expressing S247A XRCC2 mutant showed enhanced fork degradation compared with control cells (Figure 2A). Immunofluorescence staining also showed an increase in the number of pRPA32 S4/8 foci in XRCC2 S247A cells (Figure S1C), which

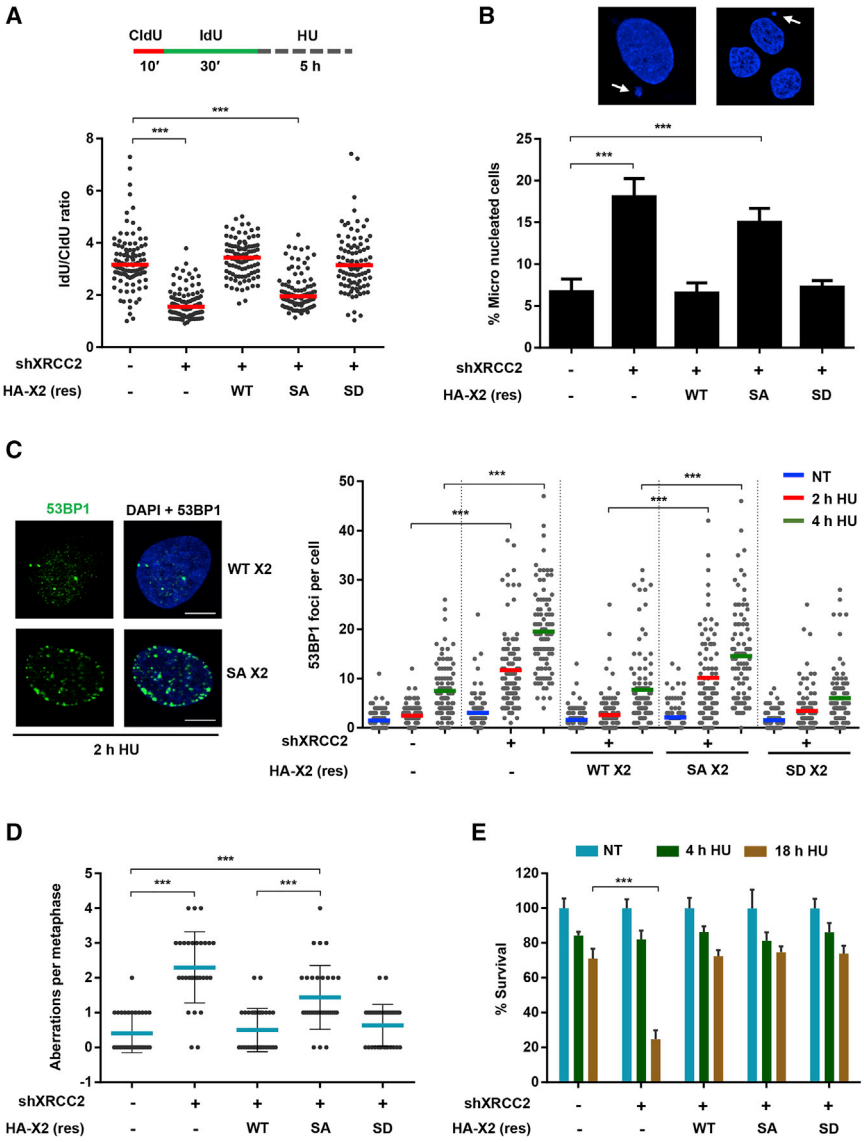

Figure 2. XRCC2 Phosphorylation Prevents the Accumulation of Replication-Associated Lesions and Promotes Genome Stability

(A) IdU-to-CldU ratios in indicated U2OS cells to study fork degradation following HU treatment (4 mM). DNA fiber labeling protocol is shown.

(B) Representative images and quantification of micronuclei in indicated U2OS cells after treatment with HU (150 μM) for 24 h. Data are presented as mean ± SD.

(C) Representative images and quantification of 53BP1 foci in indicated U2OS cells. Cells were treated with 2 mM HU for indicated times prior to pre-extraction, fixation, and immunofluorescence staining.

(D) Analysis of chromosomal aberrations in indicated U2OS cells upon 2 mM HU treatment for 2 h. Data are presented as mean ± SD.

(E) Survival of indicated U2OS cells upon exposure to 2 mM HU for 4 or 18 h. Data are representative of three independent experiments and presented as mean ± SD.

Student's t test, *p < 0.05, **p < 0.01, and ***p < 0.001; n.s., non-significant. All scale bars: 10 μm. HA-X2 (res), shRNA-resistant HA-tagged XRCC2.

serves as a marker for DNA resection. Moreover, the intensity of γH2AX in XRCC2 S247A cells increased immensely upon HU treatment, indicating high levels of replication stress (Figure S1D). Cells defective in fork protection pathway exhibit an increase in under-replicated DNA, which can ultimately manifest as chromosome breakage and micronuclei (Naim and Rosselli, 2009). We observed that XRCC2 S247A cells showed significantly more micronucleation than WT cells (Figure 2B), further confirming that XRCC2 phosphorylation is crucial for resolving replication stress. Notably, XRCC2 phospho-defective cells were proficient for HU-induced CHK1 S345 phosphorylation (Figure S2A) and regulation of origin firing (Figure S2B), indicating that activation of the ATR-CHK1 axis remains unaffected by the loss of XRCC2 phosphorylation. Collectively, these results indicate that ATR-mediated phosphorylation of XRCC2 is critical to protect nascent DNA and limit replication-associated damage during replication stress.

Unrepaired ssDNA gaps behind replication forks are likely to undergo breakage and can give rise to pathological DNA structures, including DSBs (Abe et al., 2018; Toledo et al., 2013). To test whether fork degradation in XRCC2 phospho-defective cells is associated with generation of DNA breaks, we studied 53BP1 foci formation as a marker for DSBs in U2OS cells upon HU treatment. Interestingly, XRCC2 S247A cells exhibited a severe increase in 53BP1 foci at merely 2 h of HU treatment (Figure 2C). This was confirmed by neutral comet assay, which showed significant DSB generation in XRCC2 S247A cells upon HU treatment (Figure S2C). Generation of DSBs at stalled replication forks leads to a switch in the DNA damage response from ATR to ATM kinase (Dungrawala et al., 2015; Sirbu et al., 2013; Toledo et al., 2013). ATM coordinates a signaling pathway through the RNF8 and RNF168 ubiquitin ligases, leading to ubiquitin conjugates at DSB sites (Altmeyer and Lukas, 2013a, 2013b), which can be scored using FK2 antibody. XRCC2 S247A cells displayed significantly higher intensity of FK2 than WT cells (Figures S2D and S2E) after a short pulse of HU, further supporting the notion that cells defective in XRCC2 phosphorylation undergo premature induction of DSBs during mild replication stress. Similar results were obtained in XRCC2-depleted MCF7 cells complemented with WT, S247A, or S247D XRCC2 (Figures S3A–S3D). Furthermore, U2OS cells depleted with XRCC2 or expressing the S247A mutant showed increased chromosomal aberrations following treatment with HU (Figures 2D and S2F). Thus,

XRCC2 phosphorylation is crucial for maintaining genome stability in response to replication stress.

Next, we asked whether the increased fork breakage and chromosome instability in XRCC2 S247A cells culminates in cell death. Hence, we studied cell survival in U2OS cells after exposure to different durations of HU treatment: 4 h, which induces replication stress, and 18 h, which causes global fork collapse and DSBs (Petermann et al., 2010). As expected, XRCC2-depleted cells exhibited sensitivity to prolonged HU treatment (18 h), given the role of XRCC2 in HR-mediated DSB repair (Johnson et al., 1999; Nagaraju et al., 2009). However, we failed to observe a survival defect in XRCC2-depleted cells upon short HU treatment (4 h) (Figure 2E). This observation is consistent with our previous results in Chinese hamster cells, in which *RAD51C*$^{-/-}$ and *XRCC3*$^{-/-}$ but not *XRCC2*$^{-/-}$ cells showed hypersensitivity to a short pulse of HU (Somyajit et al., 2015). Moreover, XRCC2 S247A mutants showed no survival defect at 4 or 18 h HU treatment (Figure 2E), the latter observation being consistent with our earlier report that XRCC2 phosphorylation is dispensable for HR (Saxena et al., 2018). Together, these results affirm the role of XRCC2 phosphorylation in limiting replication-associated DNA damage and genome instability during replication stress. However, loss of XRCC2 phosphorylation is competent with cell survival.

ATR Signaling Differentially Regulates XRCC2 and XRCC3

ATR kinase is the master regulator of cellular response to DNA replication stress (Cimprich and Cortez, 2008; Flynn and Zou, 2011). This is orchestrated through coordinated signaling events, involving phosphorylation of hundreds of substrates, which regulate origin firing (Toledo et al., 2013), maintenance of stalled forks (Branzei and Foiani, 2010) and various other aspects of DNA replication and repair (Cortez, 2015; Flynn and Zou, 2011). Moreover, there is now emerging evidence for the involvement of ATR in modulating replication fork progression upon stress (Lossaint et al., 2013; Mutreja et al., 2018; Saxena et al., 2018). XRCC2 is phosphorylated by ATR in response to dNTP pool alterations, and this event is crucial for restraining fork progression (Saxena et al., 2018). However, whether this activation of XRCC2 is specific only to replication stress remains obscure. To test this, we analyzed XRCC2 phosphorylation following HU-induced nucleotide pool depletion and camptothecin (CPT)-induced DSBs. Strikingly, we found that HU but not CPT led to the phosphorylation of XRCC2 on serine residues (Figure S3E), suggesting replication stress-responsive activation of XRCC2. Consistent with this, treatment with the ionizing radiation (IR)-mimetic drug zeocin failed to induce XRCC2 S247 phosphorylation (Figure 3A). Treatment with an ATM inhibitor (KU55933) led to a drastic loss of zeocin-induced pCHK2 T68 and pKAP1 S824 but caused no significant change in HU-induced XRCC2 phosphorylation (Figure 3A), suggesting that ATM is not involved in the activation of XRCC2. Collectively, these results show that XRCC2 is phosphorylated in an ATR-mediated pathway specifically in response to replication stress.

We have previously shown that XRCC3 is phosphorylated by ATR kinase specifically in response to DSBs, and its activation is crucial for DNA damage signaling and repair (Somyajit et al., 2013). Consistent with this, we observed significant XRCC3 S225 phosphorylation upon exposure to DSB-inducing drug, etoposide (Figure 3B). However, in agreement with our results from CPT and zeocin, no detectable XRCC2 phosphorylation was observed under these conditions (Figure 3B). To further validate this differential activation of XRCC2 and XRCC3, we used HU as a model agent to study the transition from fork stalling to collapse. HU-stalled replication forks remain stable in the early hours of treatment but progressively collapse into DSBs between 12 and 24 h (Petermann and Helleday, 2010; Petermann et al., 2010; Somyajit et al., 2015). Indeed, while XRCC2 phosphorylation reached a peak at 4 h of HU treatment, XRCC3 phosphorylation was evident only after 24 h of treatment (Figures 3C and 3D). Collectively, these results suggest that ATR signaling differentially activates individual RAD51 paralogs in response to distinct types of genotoxic insults.

XRCC3 phosphorylation is crucial for RAD51 loading at the sites of DSBs and subsequent HR-mediated repair (Somyajit et al., 2013). Consistent with these observations, XRCC3-depleted U2OS cells complemented with XRCC3 S225A mutant (Figure S3F) showed a significant reduction in IR-induced RAD51 focus formation compared with WT XRCC3-expressing cells (Figure S3G). No significant changes were observed in the cell cycle profiles upon expression of XRCC3 variants (Figure S3H), indicating that the difference in RAD51 foci formation was not a result of cell cycle alterations. In contrast, XRCC2 S247A mutant was found to be completely proficient in RAD51 foci formation (Figures 3E and 3F). To further explore the differential roles of XRCC2 and XRCC3 phosphorylation in genome stability, we studied replication tracts in these cells using DNA fiber assays. Replication rates were comparable in unchallenged cells (Figure S4A). However, unlike XRCC2 S247A mutants, cells defective in XRCC3 phosphorylation were found to be proficient in fork slowdown (Figure S4B) and nascent DNA protection during replication stress (Figure S4C). Together, these results show that disparate activation of the two RAD51 paralog complexes by ATR signaling ensures efficient DNA repair and genome stability upon different kinds of genotoxic stress.

XRCC3 Activation Promotes Cell Survival and Repair of Replication-Born Lesions in Cells Defective for XRCC2 Phosphorylation

It was intriguing that despite accumulation of replication-associated lesions, XRCC2 phospho-defective cells showed no survival defect upon short HU exposure. This was suggestive of the activation of a backup pathway involved in the timely repair of accumulated damage. HR has been implicated in the post-replicative repair of ssDNA gaps and collapsed forks generated during discontinuous replication (Branzei and Szakal, 2016; Petermann et al., 2010). Given that XRCC2 S247A cells are proficient in HR, we speculated that the accumulated lesions might be subsequently repaired in a recombination-dependent manner, thus allowing cell survival. Notably,

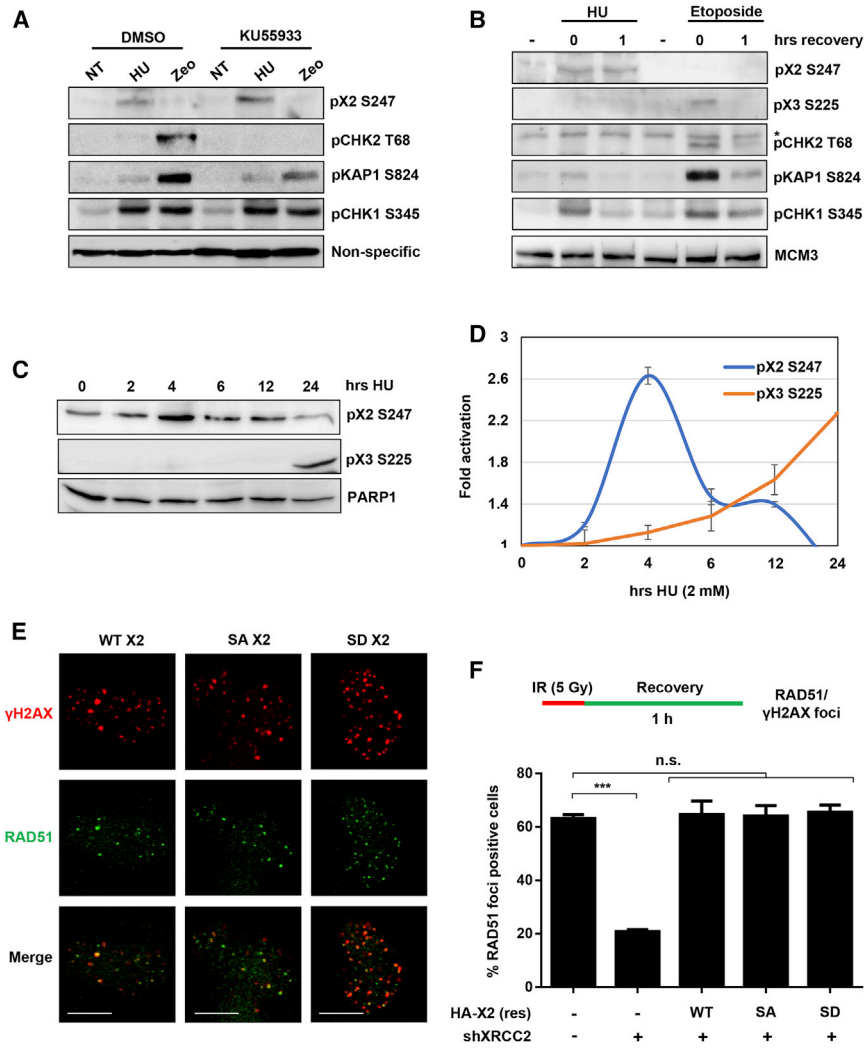

Figure 3. ATR Signaling Differentially Regulates XRCC2 and XRCC3 in Response to Replication Stress and DSBs

(A) Analysis of XRCC2 S247 phosphorylation in HeLa cells after incubation with DMSO or ATM inhibitor KU55933 (10 μM) for 1 h prior to indicated treatment (2 mM HU for 4 h or 0.5 mg/mL zeocin for 6 h). A non-specific band serves as loading control. NT, non-treated.

(B) Analysis of XRCC2 S247 and XRCC3 S225 phosphorylation in HeLa cells treated with HU (2 mM for 4 h) or etoposide (2 μM for 1 h), followed by 1 h recovery in fresh media, if indicated. MCM3 serves as loading control. Asterisk in pCHK2 blot shows a non-specific band.

(C) Analysis of XRCC2 S247 and XRCC3 S225 phosphorylation in HeLa cells treated with HU (2 mM) for indicated times. PARP-1 serves as loading control.

(D) Graph showing mean ± SD of two independent experiments for XRCC2 S247 and XRCC3 S225 phosphorylation dynamics in HeLa cells treated with HU, as shown in (C).

(E) Representative images for RAD51 foci in U2OS cells, exposed to 5 Gy IR and 1 h of recovery.

(F) Quantification of RAD51 foci-positive U2OS cells as shown in (E). Cells with more than ten RAD51 foci were considered positive. Data are presented as mean ± SD.

Student's t test, *p < 0.05, **p < 0.01, and ***p < 0.001; n.s., non-significant. All scale bars: 10 μm. HA-X2 (res), shRNA-resistant HA-tagged XRCC2.

ATM/ATR-dependent phosphorylation of XRCC3 is essential for the HR-mediated repair of collapsed replication forks induced by long HU exposure (Somyajit et al., 2013). Because XRCC2 phospho-defective cells exhibited DSB generation and activation of ATM signaling during replication stress, we reasoned that this might result in early XRCC3 activation. Indeed, XRCC2 S247A cells displayed increased XRCC3 S225 phosphorylation, beginning as early as at 2 h of HU treatment, as evident by immunofluorescence studies (Figures 4A and 4B) and immunoblotting (Figure S4D).

Next, we sought to directly investigate the role of pXRCC3-mediated HR in the repair of replication-associated DNA damage accumulated in XRCC2 S247A cells. To this end, we complemented XRCC2 and XRCC3-depleted cells with shRNA-resistant WT/S247A XRCC2 and WT/S225A XRCC3 at levels comparable with endogenous protein levels (Figures S3F and S4E). We then exposed the cells to a short HU block (4 h) and studied persisting γH2AX foci 18 h after release from HU. As expected, XRCC2 S247A cells showed an increased percentage of γH2AX-positive population, compared with WT XRCC2-expressing cells (Figure 4C). Interestingly, co-expression of S247A XRCC2 and S225A XRCC3 (double-phospho-negative cells) led to a further increase in γH2AX-positive cells upon recovery (Figure 4C), suggesting impaired repair and persistence of DNA damage. Moreover, there was a significant increase in micronucleation in the double-phospho-negative cells (Figure S4F), supporting the notion that in the absence of XRCC2 phosphorylation, ATR mediates early activation of XRCC3 to promote HR-mediated repair of accumulated DNA damage.

Next, we tested whether abrogation of HR by inhibition of XRCC3 phosphorylation leads to cell death in XRCC2 phospho-defective cells during replication stress. As expected, expression of XRCC3 S225A mutant caused WT XRCC2 cells to become hypersensitive to long HU exposure, with no prominent effect on cell survival in response to short HU exposure (Figure 4D). This further confirms that although XRCC3 phosphorylation is crucial for DSB repair, it is per se functionally independent of the replication stress response. Strikingly, combined defect of XRCC2 and XRCC3 phosphorylation effectively sensitized cells to a short HU pulse (Figure 4D). Furthermore, ATR inhibition also sensitized XRCC2 S247A cells to short HU exposure (Figure S4G). Together, these observations indicate that cells defective in XRCC2 phosphorylation cause early activation of XRCC3 during replication stress in an ATM/ATR-mediated

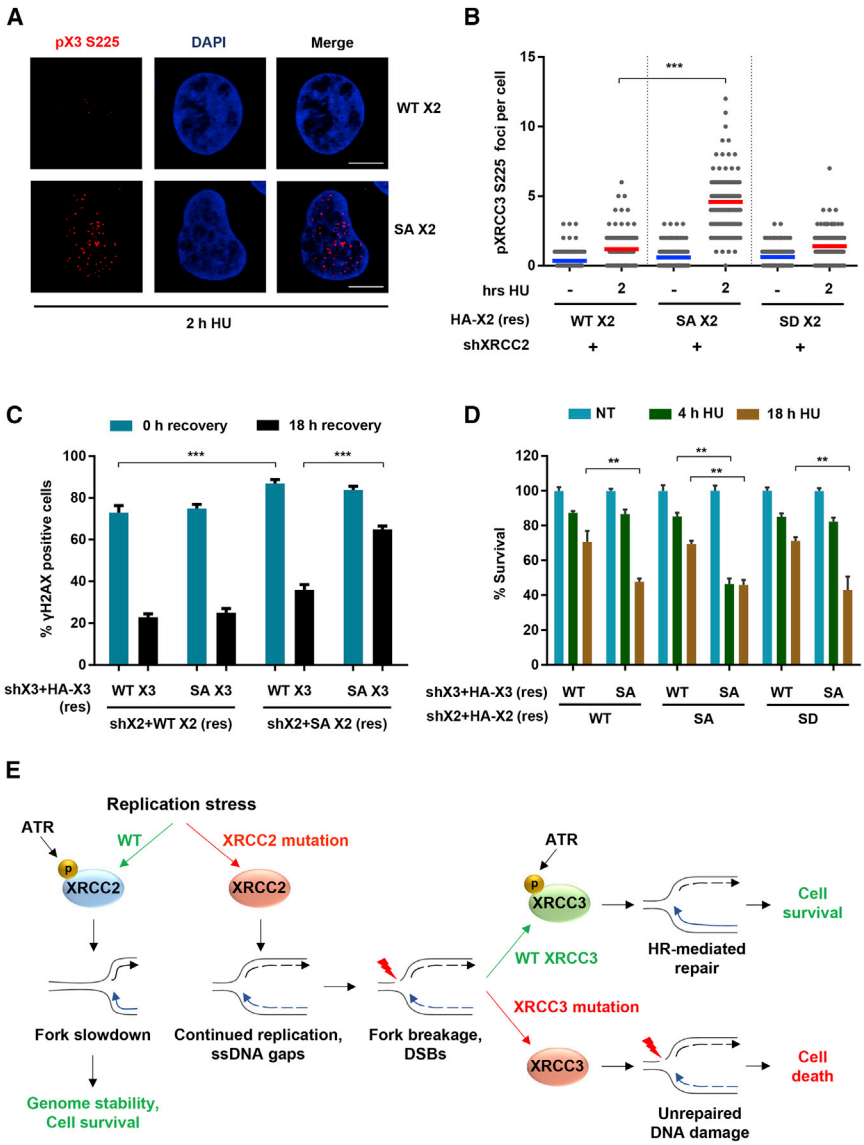

Figure 4. Early Activation of XRCC3 Facilitates Survival of XRCC2 Phospho-Defective Cells during Replication Stress

(A) Representative images for pXRCC3 S225 foci in indicated U2OS cells. Cells were treated with 2 mM HU for indicated times prior to pre-extraction, fixation, and immunofluorescence staining.

(B) Quantification of pXRCC3 S225 foci in U2OS cells as shown in (A).

(C) Quantification of γH2AX foci-positive cells. U2OS cells depleted with XRCC2 or XRCC3 and complemented with shRNA-resistant WT/S225A XRCC3 or WT/S247A XRCC2 were treated with HU (2 mM) for 4 h, followed by 18 h recovery prior to pre-extraction, fixation, and immunofluorescence staining. Cells with more than 20 foci were considered positive. Data are presented as mean ± SD.

(D) Survival of indicated U2OS cells upon exposure to 2 mM HU for 4 or 18 h. Data are representative of three independent experiments and presented as mean ± SD.

(E) Proposed model for the collaborative role of RAD51 paralogs in preventing genome instability and promoting cell survival during replication stress (see the text for discussion).

Student's t test, *$p < 0.05$, **$p < 0.01$, and ***$p < 0.001$; n.s., non-significant. All scale bars: 10 μm. HA-X2 (res), shRNA-resistant HA-tagged XRCC2; HA-X3 (res), shRNA-resistant HA-tagged XRCC3.

manner. When phosphorylated, XRCC3 facilitates recombination-mediated repair of the accumulated DNA lesions, thus promoting cell survival and genome integrity.

DISCUSSION

Here, we have identified an ATR governed pathway wherein distinct RAD51 paralogs cooperatively participate to maintain genome integrity and cell survival during replication stress. We find that cells defective in ATR-mediated phosphorylation of XRCC2 form post-replicative gaps during replication stress, resulting in increased fork processing and breakage. Consequently, these cells skew to HR-mediated DNA repair for survival, which is in turn dependent on ATM/ATR-mediated activation of XRCC3. These findings have important implications for understanding the complex interplay within this family of conserved proteins, in which each RAD51 paralog has a distinct yet collaborative role in genome maintenance, depending on the type and extent of DNA damage.

An important implication of our study is that ATR functions at multiple stages to ensure genome stability and cell survival during replication stress, depending on the extent of damage incurred by the forks. First, ATR promotes fork slowdown through XRCC2 phosphorylation. This is crucial for the "prevention" of DNA damage by limiting aberrant DNA replication and formation of ssDNA gaps in the post-replicative genome (Figure 4E). However, in the absence of this first line of defense, as in cells harboring mutations in XRCC2, forks undergo breakage, resulting in the formation of DSBs. This poises ATR for the second stage of "repair," wherein it activates XRCC3 and promotes recombination-mediated repair of the accumulated DNA damage (Figure 4E). This model is consistent with previous studies suggesting that prevention of fork collapse represents an early response of ATR to perturbed DNA replication (Chanoux et al., 2009; Couch et al., 2013). However, our results further extend these observations to propose a layered checkpoint response within the ATR pathway to limit DNA damage upon replication stress. In a similar scenario, a recent study showed that BRCA1-deficient cancer cells sequentially bypass their HR and fork protection functions during the acquisition of PARPi resistance. Notably, this rewiring is mediated by ATR, thus rendering these cells increasingly dependent on ATR for

survival (Yazinski et al., 2017). Considering these observations, our findings suggest that RAD51 paralogs might also be crucial mediators of this pathway. Moreover, given the complexity of ATR network and the functional and physical interactions among RAD51 paralogs, it is tempting to speculate that other combinations of synthetic interactions might also exist among these groups of proteins.

HR is known to play a key role in resolving spontaneous DNA damage originating in the S phase. Consistent with this, a recent study showed that loss of HR function of BRCA2 is associated with elevated replication stress, ssDNA lesions in G2, and under-replicated DNA (Feng and Jasin, 2017). Multiple types of DNA lesions including DSBs and stalled/collapsed replication forks can induce spontaneous recombination; however, there is evidence that collapsed replication forks are the most common spontaneous substrates for HR (Saleh-Gohari et al., 2005). In accordance with these studies, we find that global fork breakage in cells defective in XRCC2 phosphorylation triggers HR, as evident by the activation of XRCC3. Moreover, enhanced persistence of γH2AX foci and micronuclei were observed in cells defective in the phosphorylation of both XRCC2 and XRCC3, supporting the notion that HR acts as a salvage pathway for the repair of replication-born DNA lesions. It is likely that absence of HR might further skew these cells to alternative, potentially error-prone DSB repair mechanisms, thus creating mutagenic translocation events (Ochs et al., 2016; Willis et al., 2017). Further studies will be required to identify these pathways and understand their potential contribution to genome instability during replication stress.

Recent studies demonstrated a dependency of BRCA1/2-deficient tumors on compensatory fork maintenance functions of FANCD2 for cellular survival (Kais et al., 2016; Michl et al., 2016). Interestingly, similar to XRCC2, FANCD2 is also implicated in fork protection and genome maintenance by facilitating fork slowdown during dNTP pool depletion (Lossaint et al., 2013). In light of these observations, together with our results showing the importance of HR pathway for the survival of XRCC2 mutant cells, we propose the existence of an inverse compensatory mechanism, wherein HR proteins such as BRCA1/2 could compensate for the deficiency of fork regulation proteins such as XRCC2/FANCD2. Thus, one would expect that genetic alterations affecting primary replication stress response pathways, in combination with defective HR, would result in heightened sensitivity to chemotherapeutic strategies employing replication stress. Further identification and validation of such synthetic relationships can help in the development of novel approaches for targeted cancer therapy.

Despite their identification and initial characterization almost three decades ago (Fuller and Painter, 1988; Jones et al., 1987), the molecular mechanisms for genome maintenance and tumor suppression by mammalian RAD51 paralogs have not been clearly defined. There is some evidence suggesting that the two paralog complexes are involved in distinct functions during replication stress response and DSB repair (Chun et al., 2013; Saxena et al., 2018; Somyajit et al., 2013). Notably, double deletion involving BCDX2 and CX3 complexes was found to have an additive effect on the sensitivity to DSB-inducing agents in chicken DT40 cells (Yonetani et al., 2005), suggesting that the paralog complexes function cooperatively to promote genome stability and cell survival. In support of this notion, we find that combined defect in XRCC2 and XRCC3 phosphorylation leads to persistent DNA damage and hyper-sensitizes cells to replication stress. Moreover, our results suggest the involvement of RAD51 paralogs in a layered DNA damage response pathway governed by ATR signaling. Together, these observations not only expand the current model for genome maintenance by RAD51 paralogs but also inspire their assessment as potential targets for cancer therapy from a translational perspective.

STAR★METHODS

Detailed methods are provided in the online version of this paper and include the following:

- KEY RESOURCES TABLE
- LEAD CONTACT AND MATERIALS AVAILABILITY
- EXPERIMENTAL MODEL AND SUBJECT DETAILS
  - Cell lines
- METHOD DETAILS
  - Cell culture
  - DNA constructs and transfections
  - DNA fiber spreads
  - S1 nuclease sensitivity assay
  - Western blotting
  - Immunoprecipitation
  - Cell cycle analysis
  - Cell survival assay
  - Metaphase spreads
  - Immunofluorescence
  - Neutral comet assay
- QUANTIFICATION AND STATISTICAL ANALYSIS
- DATA AND CODE AVAILABILITY

SUPPLEMENTAL INFORMATION

Supplemental Information can be found online at https://doi.org/10.1016/j.celrep.2019.09.008.

ACKNOWLEDGMENTS

We thank IISc confocal microscopy and fluorescence-activated cell sorting (FACS) facility for their help. We greatly acknowledge funding from the Department of Science and Technology (EMR/2015/001720); the Department of Biotechnology (DBT) (BT/PR23498/BRB/10/1590/2017); a DBT-National Bioscience Award (BT/HRD/NBA/37/01/2015); the IISc-DBT partnership program (DBT/BF/PR/INS/IISc/2011–12 and BT/PR27952/INF/22/212/2018), India; and infrastructure support provided by funding from DST and UGC, India. S.S. and S.D. are supported by fellowships from the IISc and CSIR, respectively. K.S. was supported by a fellowship from the CSIR, India; a Bristol-Myers Squibb fellowship, UK, and the Ranbaxy Science Foundation, India.

AUTHOR CONTRIBUTIONS

S.S., K.S., and G.N. conceived the project and designed the experiments. S.S. and K.S. performed the experiments. S.D. contributed to the generation of reagents. S.S., K.S., and G.N. analyzed the data. S.S. and G.N. wrote the manuscript.

DECLARATION OF INTERESTS

The authors declare no competing interests.

Received: February 19, 2019
Revised: July 31, 2019
Accepted: September 4, 2019
Published: October 15, 2019

REFERENCES

Abe, T., Kawasumi, R., Giannattasio, M., Dusi, S., Yoshimoto, Y., Miyata, K., Umemura, K., Hirota, K., and Branzei, D. (2018). AND-1 fork protection function prevents fork resection and is essential for proliferation. Nat. Commun. *9*, 3091.

Altmeyer, M., and Lukas, J. (2013a). Guarding against collateral damage during chromatin transactions. Cell *153*, 1431–1434.

Altmeyer, M., and Lukas, J. (2013b). To spread or not to spread—chromatin modifications in response to DNA damage. Curr. Opin. Genet. Dev. *23*, 156–165.

Badie, S., Liao, C., Thanasoula, M., Barber, P., Hill, M.A., and Tarsounas, M. (2009). RAD51C facilitates checkpoint signaling by promoting CHK2 phosphorylation. J. Cell Biol. *185*, 587–600.

Branzei, D., and Foiani, M. (2010). Maintaining genome stability at the replication fork. Nat. Rev. Mol. Cell Biol. *11*, 208–219.

Branzei, D., and Szakal, B. (2016). DNA damage tolerance by recombination: molecular pathways and DNA structures. DNA Repair (Amst.) *44*, 68–75.

Chanoux, R.A., Yin, B., Urtishak, K.A., Asare, A., Bassing, C.H., and Brown, E.J. (2009). ATR and H2AX cooperate in maintaining genome stability under replication stress. J. Biol. Chem. *284*, 5994–6003.

Chun, J., Buechelmaier, E.S., and Powell, S.N. (2013). Rad51 paralog complexes BCDX2 and CX3 act at different stages in the BRCA1-BRCA2-dependent homologous recombination pathway. Mol. Cell. Biol. *33*, 387–395.

Cimprich, K.A., and Cortez, D. (2008). ATR: an essential regulator of genome integrity. Nat. Rev. Mol. Cell Biol. *9*, 616–627.

Cortez, D. (2015). Preventing replication fork collapse to maintain genome integrity. DNA Repair (Amst.) *32*, 149–157.

Couch, F.B., Bansbach, C.E., Driscoll, R., Luzwick, J.W., Glick, G.G., Bétous, R., Carroll, C.M., Jung, S.Y., Qin, J., Cimprich, K.A., and Cortez, D. (2013). ATR phosphorylates SMARCAL1 to prevent replication fork collapse. Genes Dev. *27*, 1610–1623.

Dungrawala, H., Rose, K.L., Bhat, K.P., Mohni, K.N., Glick, G.G., Couch, F.B., and Cortez, D. (2015). The replication checkpoint prevents two types of fork collapse without regulating replisome stability. Mol. Cell *59*, 998–1010.

Feng, W., and Jasin, M. (2017). BRCA2 suppresses replication stress-induced mitotic and G1 abnormalities through homologous recombination. Nat. Commun. *8*, 525.

Flynn, R.L., and Zou, L. (2011). ATR: a master conductor of cellular responses to DNA replication stress. Trends Biochem. Sci. *36*, 133–140.

Fuller, L.F., and Painter, R.B. (1988). A Chinese hamster ovary cell line hypersensitive to ionizing radiation and deficient in repair replication. Mutat. Res. *193*, 109–121.

Hashimoto, Y., Ray Chaudhuri, A., Lopes, M., and Costanzo, V. (2010). Rad51 protects nascent DNA from Mre11-dependent degradation and promotes continuous DNA synthesis. Nat. Struct. Mol. Biol. *17*, 1305–1311.

Johnson, R.D., Liu, N., and Jasin, M. (1999). Mammalian XRCC2 promotes the repair of DNA double-strand breaks by homologous recombination. Nature *401*, 397–399.

Jones, N.J., Cox, R., and Thacker, J. (1987). Isolation and cross-sensitivity of X-ray-sensitive mutants of V79-4 hamster cells. Mutat. Res. *183*, 279–286.

Kais, Z., Rondinelli, B., Holmes, A., O'Leary, C., Kozono, D., D'Andrea, A.D., and Ceccaldi, R. (2016). FANCD2 maintains fork stability in BRCA1/2-deficient tumors and promotes alternative end-joining DNA repair. Cell Rep. *15*, 2488–2499.

Liao, H., Ji, F., Helleday, T., and Ying, S. (2018). Mechanisms for stalled replication fork stabilization: new targets for synthetic lethality strategies in cancer treatments. EMBO Rep. *19*, e46263.

Lossaint, G., Larroque, M., Ribeyre, C., Bec, N., Larroque, C., Décaillet, C., Gari, K., and Constantinou, A. (2013). FANCD2 binds MCM proteins and controls replisome function upon activation of s phase checkpoint signaling. Mol. Cell *51*, 678–690.

Maréchal, A., and Zou, L. (2015). RPA-coated single-stranded DNA as a platform for post-translational modifications in the DNA damage response. Cell Res. *25*, 9–23.

Masson, J.Y., Tarsounas, M.C., Stasiak, A.Z., Stasiak, A., Shah, R., McIlwraith, M.J., Benson, F.E., and West, S.C. (2001). Identification and purification of two distinct complexes containing the five RAD51 paralogs. Genes Dev. *15*, 3296–3307.

Michl, J., Zimmer, J., Buffa, F.M., McDermott, U., and Tarsounas, M. (2016). FANCD2 limits replication stress and genome instability in cells lacking BRCA2. Nat. Struct. Mol. Biol. *23*, 755–757.

Mishra, A., Saxena, S., Kaushal, A., and Nagaraju, G. (2018). RAD51C/XRCC3 facilitates mitochondrial DNA replication and maintains integrity of the mitochondrial genome. Mol. Cell. Biol. *38*, e00489-17.

Mutreja, K., Krietsch, J., Hess, J., Ursich, S., Berti, M., Roessler, F.K., Zellweger, R., Patra, M., Gasser, G., and Lopes, M. (2018). ATR-mediated global fork slowing and reversal assist fork traverse and prevent chromosomal breakage at DNA interstrand cross-links. Cell Rep. *24*, 2629–2642.e5.

Nagaraju, G., Hartlerode, A., Kwok, A., Chandramouly, G., and Scully, R. (2009). XRCC2 and XRCC3 regulate the balance between short- and long-tract gene conversions between sister chromatids. Mol. Cell. Biol. *29*, 4283–4294.

Naim, V., and Rosselli, F. (2009). The FANC pathway and BLM collaborate during mitosis to prevent micro-nucleation and chromosome abnormalities. Nat. Cell Biol. *11*, 761–768.

Ochs, F., Somyajit, K., Altmeyer, M., Rask, M.B., Lukas, J., and Lukas, C. (2016). 53BP1 fosters fidelity of homology-directed DNA repair. Nat. Struct. Mol. Biol. *23*, 714–721.

Peng, M., Cong, K., Panzarino, N.J., Nayak, S., Calvo, J., Deng, B., Zhu, L.J., Morocz, M., Hegedus, L., Haracska, L., and Cantor, S.B. (2018). Opposing Roles of FANCJ and HLTF protect forks and restrain replication during stress. Cell Rep. *24*, 3251–3261.

Petermann, E., and Helleday, T. (2010). Pathways of mammalian replication fork restart. Nat. Rev. Mol. Cell Biol. *11*, 683–687.

Petermann, E., Orta, M.L., Issaeva, N., Schultz, N., and Helleday, T. (2010). Hydroxyurea-stalled replication forks become progressively inactivated and require two different RAD51-mediated pathways for restart and repair. Mol. Cell *37*, 492–502.

Quinet, A., Martins, D.J., Vessoni, A.T., Biard, D., Sarasin, A., Stary, A., and Menck, C.F. (2016). Translesion synthesis mechanisms depend on the nature of DNA damage in UV-irradiated human cells. Nucleic Acids Res. *44*, 5717–5731.

Quinet, A., Carvajal-Maldonado, D., Lemacon, D., and Vindigni, A. (2017a). DNA fiber analysis: mind the gap!. Methods Enzymol. *591*, 55–82.

Quinet, A., Lemaçon, D., and Vindigni, A. (2017b). Replication fork reversal: players and guardians. Mol. Cell *68*, 830–833.

Rickman, K., and Smogorzewska, A. (2019). Advances in understanding DNA processing and protection at stalled replication forks. J. Cell Biol. *218*, 1096–1107.

Saleh-Gohari, N., Bryant, H.E., Schultz, N., Parker, K.M., Cassel, T.N., and Helleday, T. (2005). Spontaneous homologous recombination is induced by collapsed replication forks that are caused by endogenous DNA single-strand breaks. Mol. Cell. Biol. *25*, 7158–7169.

Saxena, S., Somyajit, K., and Nagaraju, G. (2018). XRCC2 regulates replication fork progression during dNTP alterations. Cell Rep. *25*, 3273–3282.e6.

Schlacher, K., Christ, N., Siaud, N., Egashira, A., Wu, H., and Jasin, M. (2011). Double-strand break repair-independent role for BRCA2 in blocking stalled replication fork degradation by MRE11. Cell *145*, 529–542.

Schlacher, K., Wu, H., and Jasin, M. (2012). A distinct replication fork protection pathway connects Fanconi anemia tumor suppressors to RAD51-BRCA1/2. Cancer Cell *22*, 106–116.

Sirbu, B.M., McDonald, W.H., Dungrawala, H., Badu-Nkansah, A., Kavanaugh, G.M., Chen, Y., Tabb, D.L., and Cortez, D. (2013). Identification of proteins at active, stalled, and collapsed replication forks using isolation of proteins on nascent DNA (iPOND) coupled with mass spectrometry. J. Biol. Chem. *288*, 31458–31467.

Somyajit, K., Subramanya, S., and Nagaraju, G. (2010). RAD51C: a novel cancer susceptibility gene is linked to Fanconi anemia and breast cancer. Carcinogenesis *31*, 2031–2038.

Somyajit, K., Subramanya, S., and Nagaraju, G. (2012). Distinct roles of FANCO/RAD51C protein in DNA damage signaling and repair: implications for Fanconi anemia and breast cancer susceptibility. J. Biol. Chem. *287*, 3366–3380.

Somyajit, K., Basavaraju, S., Scully, R., and Nagaraju, G. (2013). ATM- and ATR-mediated phosphorylation of XRCC3 regulates DNA double-strand break-induced checkpoint activation and repair. Mol. Cell. Biol. *33*, 1830–1844.

Somyajit, K., Saxena, S., Babu, S., Mishra, A., and Nagaraju, G. (2015). Mammalian RAD51 paralogs protect nascent DNA at stalled forks and mediate replication restart. Nucleic Acids Res. *43*, 9835–9855.

Somyajit, K., Gupta, R., Sedlackova, H., Neelsen, K.J., Ochs, F., Rask, M.B., Choudhary, C., and Lukas, J. (2017). Redox-sensitive alteration of replisome architecture safeguards genome integrity. Science *358*, 797–802.

Suwaki, N., Klare, K., and Tarsounas, M. (2011). RAD51 paralogs: roles in DNA damage signalling, recombinational repair and tumorigenesis. Semin. Cell Dev. Biol. *22*, 898–905.

Técher, H., Koundrioukoff, S., Nicolas, A., and Debatisse, M. (2017). The impact of replication stress on replication dynamics and DNA damage in vertebrate cells. Nat. Rev. Genet. *18*, 535–550.

Toledo, L.I., Altmeyer, M., Rask, M.B., Lukas, C., Larsen, D.H., Povlsen, L.K., Bekker-Jensen, S., Mailand, N., Bartek, J., and Lukas, J. (2013). ATR prohibits replication catastrophe by preventing global exhaustion of RPA. Cell *155*, 1088–1103.

Toledo, L., Neelsen, K.J., and Lukas, J. (2017). Replication catastrophe: when a checkpoint fails because of exhaustion. Mol. Cell *66*, 735–749.

Wiese, C., Collins, D.W., Albala, J.S., Thompson, L.H., Kronenberg, A., and Schild, D. (2002). Interactions involving the Rad51 paralogs Rad51C and XRCC3 in human cells. Nucleic Acids Res. *30*, 1001–1008.

Willis, N.A., Frock, R.L., Menghi, F., Duffey, E.E., Panday, A., Camacho, V., Hasty, E.P., Liu, E.T., Alt, F.W., and Scully, R. (2017). Mechanism of tandem duplication formation in BRCA1-mutant cells. Nature *551*, 590–595.

Yazinski, S.A., Comaills, V., Buisson, R., Genois, M.M., Nguyen, H.D., Ho, C.K., Todorova Kwan, T., Morris, R., Lauffer, S., Nussenzweig, A., et al. (2017). ATR inhibition disrupts rewired homologous recombination and fork protection pathways in PARP inhibitor-resistant BRCA-deficient cancer cells. Genes Dev. *31*, 318–332.

Yonetani, Y., Hochegger, H., Sonoda, E., Shinya, S., Yoshikawa, H., Takeda, S., and Yamazoe, M. (2005). Differential and collaborative actions of Rad51 paralog proteins in cellular response to DNA damage. Nucleic Acids Res. *33*, 4544–4552.

Zeman, M.K., and Cimprich, K.A. (2014). Causes and consequences of replication stress. Nat. Cell Biol. *16*, 2–9.

Zheng, Z., Ng, W.L., Zhang, X., Olson, J.J., Hao, C., Curran, W.J., and Wang, Y. (2012). RNAi-mediated targeting of noncoding and coding sequences in DNA repair gene messages efficiently radiosensitizes human tumor cells. Cancer Res. *72*, 1221–1228.

STAR★METHODS

KEY RESOURCES TABLE

REAGENT or RESOURCE	SOURCE	IDENTIFIER
Antibodies		
Rat anti-BrdU antibody	Abcam	Cat# ab6326; RRID: AB_305426
Donkey Anti-Rat Alexa Fluor® 594	Abcam	Cat# ab150156
Purified Mouse Anti-BrdU	BD Biosciences	Cat# 347580: RRID: AB_400326
Rabbit Anti-Mouse IgG H&L (Alexa Fluor® 488)	Abcam	Cat# ab150125
Anti-XRCC2	Santa Cruz	Cat# sc-365854: RRID: AB_10846464
Anti- XRCC3	Santa Cruz	Cat# sc-271714: RRID: AB_10708416
Anti- RPA70	Abcam	Cat# ab79398: RRID: AB_1603759
Anti- BrdU	BD Biosciences	Cat# 555627: RRID: AB_10015222
Anti- HA tag	Roche	Cat# 10952100
Anti- pKAP1 S824	Abcam	Cat# ab70369: RRID: AB_1209417
Anti- pCHK1 S345	Abcam	Cat# ab58567: RRID: AB_10563825
Anti- pCHK1 S345	Cell Signaling Technology	Cat# 2348S: RRID: AB_331212
Anti- CHK1	Santa Cruz	Cat# sc-377231
Anti- pCHK2 T68	Abcam	Cat# ab85743: RRID: AB_10858765
Anti- pCHK2 T68	Cell Signaling Technology	Cat# 2197S: RRID: AB_2080501
Anti- MCM3	Santa Cruz	Cat# sc-365616: RRID: AB_10846721
Anti- RAD51	Santa Cruz	Cat# sc-8349: RRID: AB_2253533
Anti- HSP90	Santa Cruz	Cat# sc-69703: RRID: AB_2121191
Anti- 53BP1	Millipore	Cat# 05-725: RRID: AB_309939
Anti-Ubiquitinylated proteins, clone FK2 antibody	Millipore	Cat# 04-263: RRID: AB_612093
Anti- H2AX (pS139)	BD Biosciences	Cat# 560443: RRID: AB_1645592
Anti- Phospho RPA32 (S4/S8)	Bethyl	Cat# A300-245A: RRID: AB_210547
Anti- Phospho Serine	Thermo Fisher Scientific	Cat# 61-8100: RRID: AB_2533940
Anti- PARP1	Santa Cruz	Cat# sc-365315: RRID: AB_10842296
Anti- pXRCC3 S225	Somyajit et al., 2013	N/A
Anti- pXRCC2 S247	Saxena et al., 2018	N/A
Chemicals, Peptides, and Recombinant Proteins		
5-Chloro-2′-deoxyuridine	Sigma-Aldrich	Cat# C6891
5-Iodo-2′-deoxyuridine	Sigma-Aldrich	Cat# I7125
5-Bromo-2′-deoxyuridine	Sigma-Aldrich	Cat# B5002
Hydroxyurea	Sigma-Aldrich	Cat# H8627
DAPI	Sigma-Aldrich	Cat# D8417
Camptothecin	Sigma-Aldrich	Cat# C9911
S1 nuclease	Invitrogen	Cat# 18001016
Propidium iodide	Sigma-Aldrich	Cat# P4170
cOmplete, Mini Protease Inhibitor Cocktail	Roche	Cat# 11836153001
PhosSTOP	Roche	Cat# 4906837001
Thiazolyl Blue Tetrazolium Bromide (MTT reagent)	Sigma-Aldrich	Cat# M2128
VE821 (ATR inhibitor)	Selleckchem	Cat# 8007
KaryoMAX Colcemid Solution	Thermo Fisher Scientific	Cat# 15212012
G 418 Sulfate	Calbiochem	Cat# 108321-42-2

(*Continued on next page*)

Continued

REAGENT or RESOURCE	SOURCE	IDENTIFIER
Deposited Data		
Raw imaging and western data	This paper	https://data.mendeley.com/datasets/ycfy5yv79c/draft?a=1677a562-6ea5-425b-8268-c9591e5897d9
Experimental Models: Cell Lines		
U2OS	ATCC	HTB-96
MCF7	ATCC	HTB-22
HeLa	ATCC	CCL-2
Oligonucleotides		
shXRCC2#1 (5′-TTGCAACGACACAAACTATAA-3′)	Sigma-Aldrich	N/A
shXRCC3#1 (5′-GAATTATTGCTGCAATTAA-3′)	Sigma-Aldrich	N/A
XRCC2 primers (Refer to Table S1)	N/A	N/A
XRCC3 primers (Refer to Table S1)	N/A	N/A
Recombinant DNA		
pcDNA3β-HA WT XRCC2	Somyajit et al., 2015 Saxena et al., 2018	N/A
pcDNA3β-HA WT XRCC2 (shXRCC2#1 resistant)	Saxena et al., 2018	N/A
pcDNA3β-HA S247A XRCC2 (shXRCC2#1 resistant)	Saxena et al., 2018	N/A
pcDNA3β-HA S247D XRCC2(shXRCC2#1 resistant)	Saxena et al., 2018	N/A
pcDNA3β-HA WT XRCC3 (shXRCC3#1 resistant)	This paper	N/A
pcDNA3β-HA S225A XRCC3 (shXRCC3#1 resistant)	This paper	N/A
Software and Algorithms		
GraphPad Prism 6	GraphPad Software	https://www.graphpad.com/
ImageJ (DNA fiber length analysis)	ImageJ Software	https://imagej.nih.gov/ij/
FACSDiva Version 6.1.1 software	Becton Dickinson	N/A
ImageQuant LAS 4000	GE healthcare	N/A
Leica Application Suite (LAS) Advanced software	Leica microsystems	N/A

LEAD CONTACT AND MATERIALS AVAILABILITY

Further information and requests for resources and reagents should be directed to and will be fulfilled by the Lead Contact, Prof. Ganesh Nagaraju (nganesh@iisc.ac.in). All plasmids and unique/stable reagents generated in this study are available on request without restrictions.

EXPERIMENTAL MODEL AND SUBJECT DETAILS

Cell lines

Human cell lines U2OS, MCF7 and HeLa were obtained from ATCC. Source and identifier (if applicable) of cell lines used in this study are also listed in the key resources table.

METHOD DETAILS

Cell culture

Human cell lines U2OS, MCF7 and HeLa were grown in DMEM supplemented with 10% FBS and penicillin/streptomycin (Sigma-Aldrich) at 37°C in humidified air containing 5% CO2. For generation of stable cell lines, cells were subjected to Neomycin selection 48 h after transfection (G418 sulfate; 1.6 mg/ml). The colonies were later pooled and propagated under constant neomycin selection (0.4 mg/ml).

DNA constructs and transfections

Human XRCC2 WT, phospho-defective and phospho-mimetic constructs, shRNA resistant constructs (Saxena et al., 2018) and human XRCC3 WT, phospho-defective (Somyajit et al., 2013) and shRNA resistant constructs were generated using PCR-based

mutagenesis and cloned into pcDNA3β vector using *E. coli* DH5α. Sequences of primers used for generation of the constructs are listed in Table S1. XRCC2 and XRCC3 shRNA constructs were generated using reported siRNA sequences and cloned into pRS shRNA vector.

XRCC2#1: 5′-TTGCAACGACACAAACTATAA-3′ (Saxena et al., 2018; Zheng et al., 2012)
XRCC3#1: 5′-GAATTATTGCTGCAATTAA-3′ (Saxena et al., 2018; Somyajit et al., 2013)

All plasmid transfections for stable and transient expression were performed using a Bio-Rad gene pulsar X cell (250 V and 950 μF). 6-8 hr after transfection, fresh media was added to the cells. Cells were harvested/proceeded for indicated treatments (18-24 h after the transfection for XRCC2 and 30-36 h after the transfection for XRCC3).

DNA fiber spreads

Approximately 5 × 10^5 cells were plated in each well of a six-well plate. Cells were pulse-labeled with 25 μM CldU and 250 μM IdU as indicated in the sketches. Later, cells were harvested and re-suspended in 50 μL of chilled PBS. Cell suspensions (3 μl) were placed on glass slides (Thermo Scientific Superfrost) and briefly allowed to air-dry. The cell suspension was then mixed with 8 μL of lysis buffer (0.5% sodium dodecyl sulfate, 200 mM Tris-HCl [pH 7.4], 50 mM EDTA) and incubated for 2 min. Slides were inclined at 45° to spread the suspension. Once dried, DNA spreads were fixed by incubation in a 3:1 solution of methanol-acetic acid for 10 min, followed by denaturation with 2.5 N HCl for 80 min. After several rinses in PBS, the slides were incubated with blocking buffer (2% BSA and 0.01% Tween-20 in PBS) for 15 min. This was followed by incubation with rat anti-BrdU antibody (1:100 in blocking buffer; Abcam; ab6326) for 90 min in a humidified chamber at room temperature (RT). The slides were washed once with 0.1% Tween-20 and fixed in 4% formaldehyde solution for 15 min. After multiple PBS washes, the slides were incubated with AlexaFluor 594-conjugated Anti-Rat secondary antibody (1:100 in blocking buffer; Abcam; ab150156). After incubation for 1 h at RT, slides were washed twice with 0.1% Tween-20 and incubated overnight with mouse Anti-IdU antibody (1:25 in blocking buffer; BD Biosciences; 347580) at 4°C. Slides were washed twice with PBS and incubated with AlexaFluor 488-conjugated Anti-Mouse antibody (1:50 in blocking buffer; Abcam; 150125). After 2 washes with 0.1% Tween-20, slides were mounted with coverslips using Dabco mounting media (Sigma-Aldrich). Fibers were imaged using an Olympus IX71 microscope. Between 100 and 250 fibers were measured using ImageJ software from 2-3 independent experiments and P values were calculated using Prism software.

Effect of drug treatment on fork progression is represented as the ratio of IdU (labeled in the presence of the drug) to CldU tract lengths. For calculation of replication rate (kb/min) in unchallenged cells, length of IdU tracts (in kb) was divided by the time of IdU labeling (in minutes).

S1 nuclease sensitivity assay

The S1 nuclease assay for detection of ssDNA gaps was performed as described previously (Quinet et al., 2016, 2017a). Briefly, after the IdU pulse, cells were treated with CSK100 buffer (100 mM NaCl, 10 mM MOPS, 3 mM MgCl2 [pH 7.2], 300 mM sucrose, and 0.5% Triton X-100) for 10 min at room temperature, then incubated with S1 nuclease buffer (30 mM sodium acetate [pH 4.6], 1 mM zinc acetate, 5% glycerol, and 50 mM NaCl) with or without 20 U/mL S1 nuclease (Invitrogen, 18001-016) for 30 min at 37°C. The cells were then scraped in PBS + 0.1% BSA and centrifuged at 7,000 rpm for 5 min at 4°C. Cell pellets were resuspended in chilled PBS and proceeded for DNA fiber spreading as described before.

Western blotting

Cells were harvested and lysed in RIPA buffer (without SDS) supplemented with cOmplete and PhosSTOP tablets (Roche). Protein concentrations were estimated by standard Bradford assay. Proteins were resolved on a 10% SDS-PAGE gel and transferred onto PVDF membranes (Millipore). The membranes were blocked using 5% dry milk (w/v) in TBST (50 mM Tris-HCl pH 8.0, 150 mM NaCl, 0.1% tween-20). For analysis of phosphorylated proteins, 3% BSA (w/v) in TBST was used for blocking. The membranes were then incubated with primary antibody overnight at 4°C. The membranes were washed with TBST and incubated with respective HRP-conjugated secondary antibodies (1:8000; Santa Cruz) for 1 h at 4°C. After TBST washes, membranes were developed with chemiluminescent HRP substrate (Millipore) and imaged using Chemidoc (GE healthcare LAS 4000).

Immunoprecipitation

After harvesting, cells were washed in PBS and lysed in IP lysis buffer (150 mM NaCl, 50 mM Tris-HCl [pH 8.0], 1% NP-40, 0.5% sodium deoxy cholate, 0.1% SDS) supplemented with cOmplete and PhosSTOP tablets (Roche). After 1 h incubation on ice, lysates were cleared by centrifugation. Where appropriate, antibodies were added to lysate and incubated for 12-16 h at 4°C. Lysates were then incubated with 25 μl of Protein A/G beads (GE Healthcare) for 2 h at 4°C. Ig–antigen complexes were washed extensively and eluted in 2x Laemmli sample buffer at 90°C for 30 min before SDS-PAGE.

Cell cycle analysis

Cells were harvested and single-cell suspensions were fixed overnight with 70% ethanol in PBS at −20°C. After centrifugation, the cells were incubated with RNaseA (0.1 mg/ml) in PBS at 42°C for 4 h and then incubated for 10 min with PI (50 μg/ml) in dark. A total of

$1x10^4$ cells were analyzed by Verse flow cytometer (Becton Dickinson). Aggregates were gated out and percentage of cells with 2N and 4N DNA content was calculated using FACSDiva Version 6.1.1 software (Becton Dickinson).

Cell survival assay

Cells (5000/well) were seeded in a 24-well plate. After treatment (or mock treatment) with HU as indicated, cells were allowed to grow for 7-10 days. Cell survival was monitored by MTT (0.1 mg/ml; Sigma-Aldrich) assay using microplate reader (VersaMax ROM version 3.13). Percent cell survival was calculated as treated cells/untreated cells × 100.

Metaphase spreads

Cells were treated with HU for 4 h, recovered for 24 h in fresh media and incubated with Demecolcine (1 μg/ml) for the last 4 h of recovery. Cells were then harvested and treated with hypotonic solution (75 mM KCl) for 12 min, washed three times with chilled fixative (methanol/acetic acid 1:1), and left overnight at 4°C. Cells were later dropped onto a chilled glass slide, air-dried and visualized using Olympus CKX41 inverted microscope. For each case, at least 100 metaphase plates were scored.

Immunofluorescence

Exponentially growing cells were seeded onto coverslips, then treated (or mock-treated) with HU as indicated. After treatment, the cells were washed with PBS and fixed in 3.7% formaldehyde for 10 min at RT. If indicated, pre-extraction was performed with 0.2% Triton X-100 on ice for 90 s before fixation. Later, cells were blocked in blocking buffer (0.5% BSA and 0.5% Triton X-100 in PBS) for 30 min. For native BrdU staining, cells were incubated with 10 μM BrdU for 24 h, washed and treated with 500 μM HU for 2 h. For staining, cells were pre-extracted on ice for 2 min, followed by blocking in BrdU blocking buffer (10% FBS and 0.01% sodium azide in DMEM). The coverslips were incubated with the indicated primary antibodies for 2 h at RT. After a wash with blocking buffer, the coverslips were incubated with respective FITC/TRITC/AlexaFluor-conjugated secondary antibodies for 1 h at RT, and then stained with DAPI (1 ug/ml; Sigma-Aldrich) for 10 min before mounting onto slides. Cells were acquired using a confocal microscope (LSM510; Carl Zeiss) and images were processed using Zeiss LSM image browser software.

Neutral comet assay

24 h before the experiment, Silane-Prep Slides from Sigma (S4651-72EA) were pre-coated in 0.8% agarose in PBS and stored at R.T. Cells were treated as required, harvested in PBS, centrifuged and resuspended in 200 μl of 0.8% low melting point (LMP) agarose. 75 μl of cell-agarose suspension was spread on precoated slides, covered with coverslip and placed on icepack for 10 min for solidification. The coverslip was removed and a layer of LMP agarose was spread on the top. This was again covered with a coverslip and placed on icepack for 10 min. The coverslip was removed, and the slides were placed in chilled lysis solution (2.5 M NaCl, 0.1 M EDTA, 10 mM Tris base (pH 10),1% N-laurylsarcosine, 0.5% Triton X-100) at 4°C for 2 hr. The slides were washed three times in the electrophoresis buffer (300 mM sodium acetate and 100 mM Tris-HCl (pH 8.3)), followed by electrophoresis at 15 V (0.5 V/cm) for 1 h at R.T. The slides were washed three times in PBS, fixed in absolute ethanol and air-dried. The slides were stained with 50 μL ethidium bromide (2 μg/ml in water), covered with coverslip and imaged using an Olympus IX71 microscope. Between 70-100 comets were measured using ImageJ software with OpenComet plugin from 2 independent experiments.

QUANTIFICATION AND STATISTICAL ANALYSIS

Statistical differences in RAD51 foci experiments, chromosomal aberrations assays, cell cycle analysis were determined in terms of p value from two-tailed Student's t test. Statistics for DNA fiber and immunofluorescence data were calculated using GraphPad Prism software (Version 6.0). N (in DNA fiber data) denotes the number of fibers analyzed per condition. A minimum of 100 DNA fibers were analyzed for each condition. N (in immunofluorescence data) denotes the number of cells analyzed per condition. A minimum of 100 cells were analyzed for each condition. Values of N and P are provided in the respective figure legends.

DATA AND CODE AVAILABILITY

This study did not generate/analyze datasets/code.

Cell Reports, Volume *29*

Supplemental Information

ATR Signaling Uncouples the Role of RAD51 Paralogs in Homologous Recombination and Replication Stress Response

Sneha Saxena, Suruchi Dixit, Kumar Somyajit, and Ganesh Nagaraju

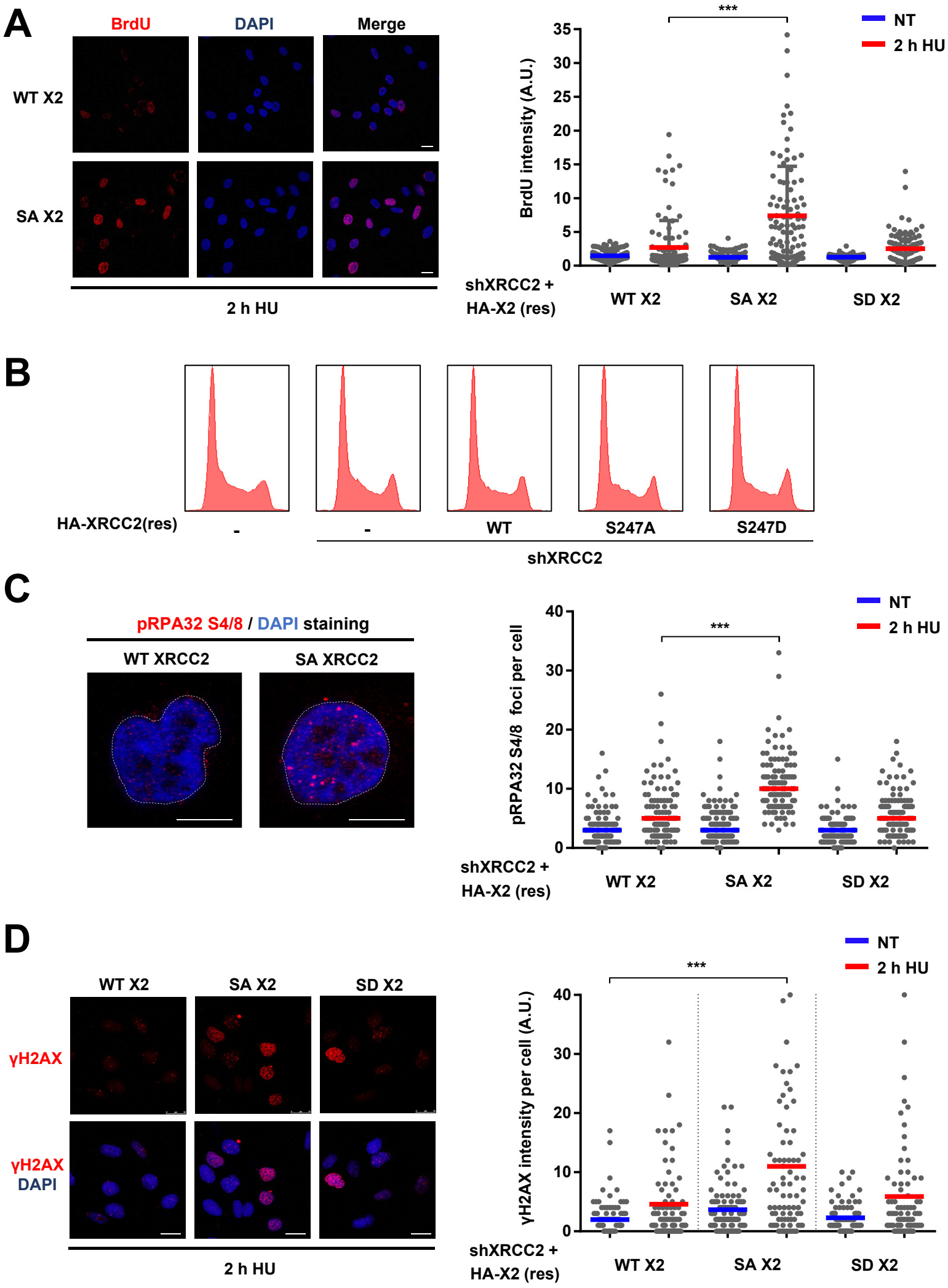
A
BrdU
DAPI
Merge
WT X2
SA X2
2 h HU
***
NT
2 h HU
BrdU intensity (A.U.)
35
30
25
20
15
10
5
0
shXRCC2 +
HA-X2 (res)
WT X2
SA X2
SD X2
B
HA-XRCC2(res)
-
-
WT
S247A
S247D
shXRCC2
C
pRPA32 S4/8 / DAPI staining
WT XRCC2
SA XRCC2
NT
2 h HU
***
pRPA32 S4/8 foci per cell
40
30
20
10
0
shXRCC2 +
HA-X2 (res)
WT X2
SA X2
SD X2
D
WT X2
SA X2
SD X2
γH2AX
γH2AX
DAPI
2 h HU
NT
2 h HU
***
γH2AX intensity per cell (A.U.)
40
30
20
10
0
shXRCC2 +
HA-X2 (res)
WT X2
SA X2
SD X2

Figure S1

Figure S1. XRCC2 phosphorylation limits the accumulation of DNA damage during mild replication stress. Related to Figures 1 and 2. (A) Representative images and quantification of XRCC2 depleted U2OS cells expressing indicated shRNA resistant XRCC2 variants stained for BrdU under non-denaturing conditions. Data are presented as mean intensity ± SD. Scale bars: 20 μm. (B) Cell cycle analysis using propidium iodide (PI) staining in U2OS cells depleted of XRCC2 and complemented with indicated shRNA resistant XRCC2 variants. (C) Representative images and quantification of XRCC2 depleted U2OS cells expressing indicated shRNA resistant XRCC2 variants stained for pRPA32 S4/8. Cells were treated with 2 mM HU for indicated times prior to pre-extraction, fixation and immunofluorescence staining. Scale bars: 10 μm. (D) Representative images and quantification of XRCC2 depleted U2OS cells expressing indicated shRNA resistant XRCC2 variants stained for γH2AX. Cells were treated with 2 mM HU for indicated times prior to pre-extraction, fixation and immunofluorescence staining. A.U., arbitrary units. Scale bars: 25 μm. HA-X2 (res), shRNA resistant HA-tagged XRCC2. Student's t-test, *$p < 0.05$; **$p < 0.01$; ***$p < 0.001$. n.s., non-significant.

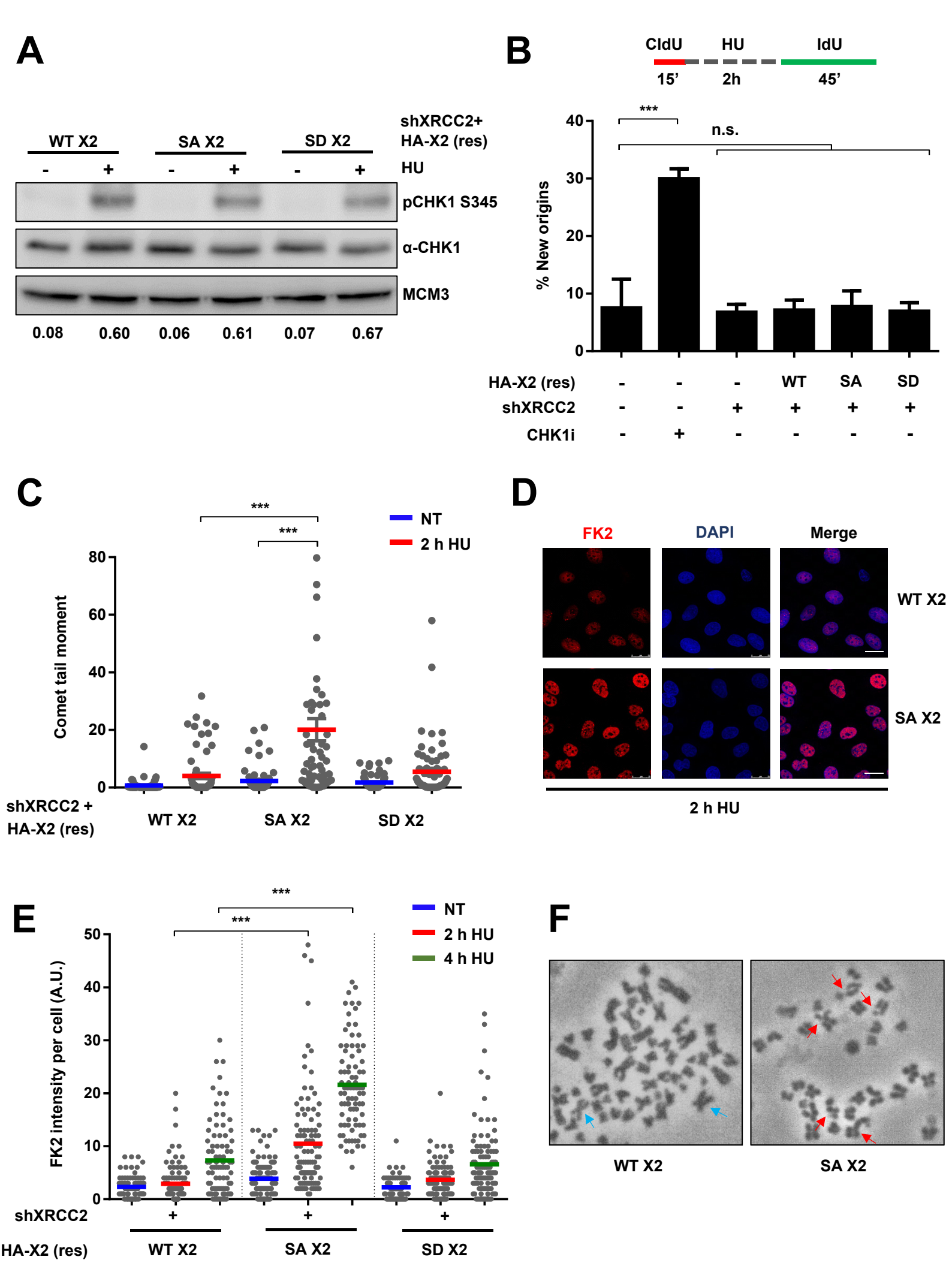
A
WT X2
SA X2
SD X2
shXRCC2+
HA-X2 (res)
- + - + - +
HU
pCHK1 S345
α-CHK1
MCM3
0.08 0.60 0.06 0.61 0.07 0.67
B
CldU
HU
IdU
15'
2h
45'
***
n.s.
% New origins
0
10
20
30
40
HA-X2 (res) - - - WT SA SD
shXRCC2 - - + + + +
CHK1i - + - - - -
C
***
***
NT
2 h HU
Comet tail moment
0
20
40
60
80
shXRCC2 +
HA-X2 (res)
WT X2
SA X2
SD X2
D
FK2
DAPI
Merge
WT X2
SA X2
2 h HU
E
***
***
NT
2 h HU
4 h HU
FK2 intensity per cell (A.U.)
0
10
20
30
40
50
shXRCC2
+ + +
HA-X2 (res)
WT X2
SA X2
SD X2
F
WT X2
SA X2

Figure S2

Figure S2. XRCC2 phosphorylation fosters genome integrity during replication stress. Related to Figure 2. (A) Western blot for pCHK1 S345 activation in indicated U2OS cells upon treatment with 2 mM HU for 4 h. Ratio of phosphorylated to total CHK1 is indicated below the respective lanes. (B) Frequency of new origin firing in indicated U2OS cells. U2OS cells were sequentially labelled with CldU and IdU with a 2 h HU pulse (2 mM) in between. Green-only tracts were counted as newly fired origins. CHK1 inhibition was included as a positive control for increased origin firing. New origins are shown as percentage of all labelled tracks. DNA fiber labeling protocol is shown. Data are presented as mean ± SD. (C) Cells were treated with 2 mM HU for indicated times and collected to perform neutral comet assay. Data are presented as mean tail moment ± SEM. (D) Representative images of XRCC2 depleted U2OS cells expressing indicated shRNA resistant XRCC2 variants stained for FK2. Cells were treated with 2 mM HU for indicated times prior to pre-extraction, fixation and immunofluorescence staining. Scale bars: 25 µm. (E) Quantification of FK2 intensity in cells as in (D). A.U., arbitrary units. HA-X2 (res), shRNA resistant HA-tagged XRCC2. (F) Representative images for metaphase spreads in XRCC2 depleted U2OS cells expressing indicated shRNA resistant XRCC2 variants. Blue and red arrows indicate normal chromosomes and chromosomal aberrations respectively. Student's t-test, *$p < 0.05$; **$p < 0.01$; ***$p < 0.001$. n.s., non-significant.

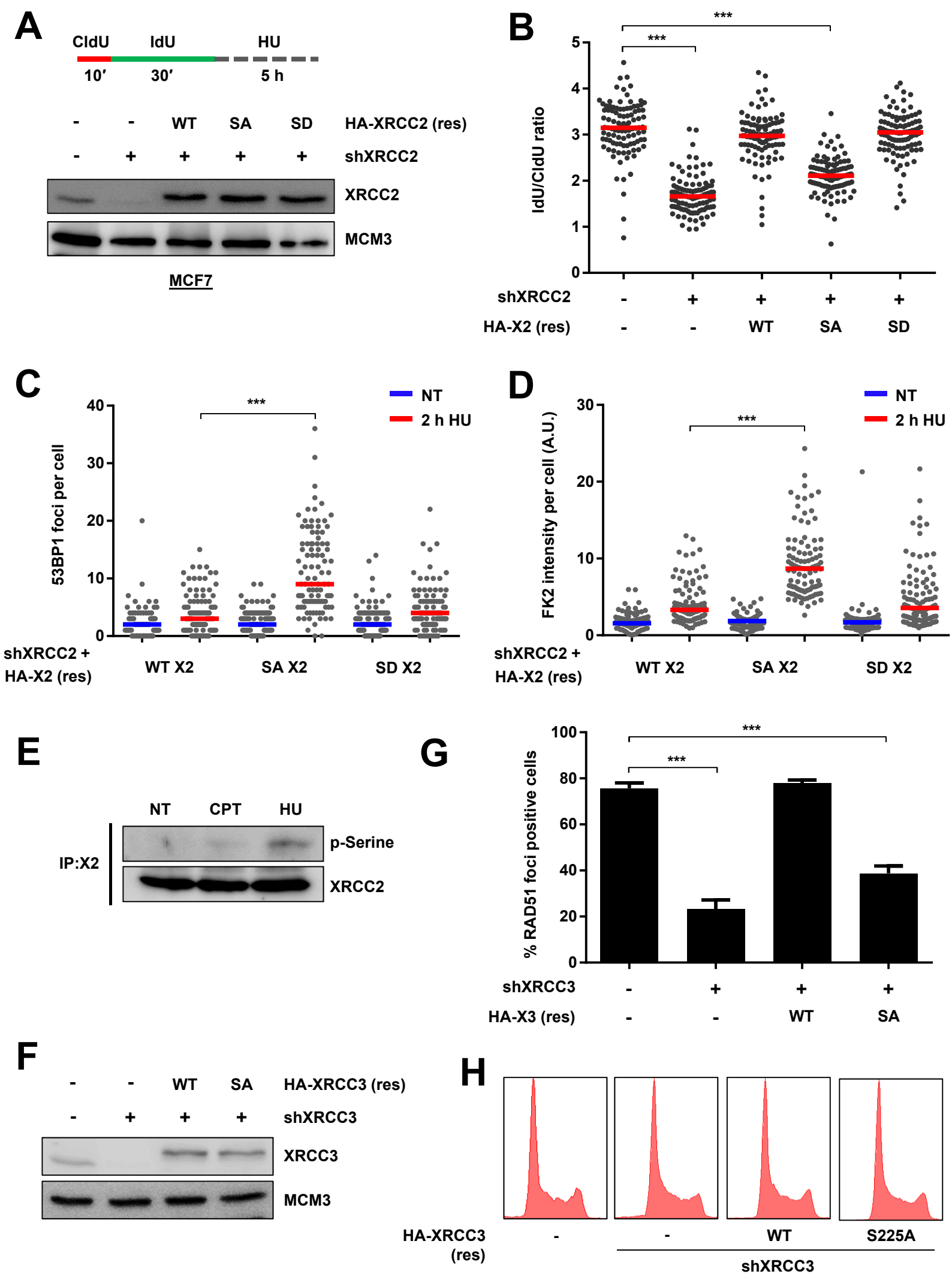
A
CldU
IdU
HU
10′
30′
5 h
- - WT SA SD HA-XRCC2 (res)
- + + + + shXRCC2
XRCC2
MCM3
MCF7
B
***
***
IdU/CldU ratio
shXRCC2 - + + + +
HA-X2 (res) - - WT SA SD
C
***
NT
2 h HU
53BP1 foci per cell
shXRCC2 +
HA-X2 (res)
WT X2
SA X2
SD X2
D
***
NT
2 h HU
FK2 intensity per cell (A.U.)
shXRCC2 +
HA-X2 (res)
WT X2
SA X2
SD X2
E
NT CPT HU
IP:X2
p-Serine
XRCC2
G
***
***
% RAD51 foci positive cells
shXRCC3 - + + +
HA-X3 (res) - - WT SA
F
- - WT SA HA-XRCC3 (res)
- + + + shXRCC3
XRCC3
MCM3
H
HA-XRCC3 (res) - - WT S225A
shXRCC3

Figure S3

Figure S3. ATR signaling uncouples the roles of RAD51 paralog complexes in replication stress response and DSB repair. Related to Figures 2 and 3. (A) Western blot shows depletion of endogenous XRCC2 and expression of shRNA-resistant HA-tagged XRCC2 variants in MCF7 cells. HA-X2 (res), shRNA resistant HA-tagged XRCC2; WT, wild-type; SA, S247A; SD, S247D. Top, Schematic to study fork degradation in MCF7 cells. (B) IdU to CldU tract length ratios in indicated MCF7 cells to study fork degradation following HU treatment (4 mM). (C and D) Quantification of 53BP1 foci (C) and FK2 intensity (D) in XRCC2 depleted MCF7 cells expressing indicated shRNA resistant XRCC2 variants. Cells were treated with 2 mM HU for indicated times prior to pre-extraction, fixation and immunofluorescence staining. A.U., arbitrary units. (E) HeLa cells were used to analyze phosphorylation of XRCC2 and where indicated, DNA damage was induced with HU (2 mM) or CPT (5 μM) for 1 h. Cell extracts were prepared and immunoprecipitated (IP) using XRCC2 antibody. Following IP, the proteins were immunoblotted with indicated antibodies. (F) Western blot shows depletion of endogenous XRCC3 and expression of shRNA-resistant HA-tagged XRCC3 variants in U2OS cells. HA-XRCC3 (res), shRNA resistant HA-tagged XRCC3; WT, wild-type; SA, S225A. (G) Quantification of RAD51 foci positive cells in XRCC3 depleted U2OS cells expressing shRNA resistant HA-tagged WT/S225A XRCC3, exposed to 5 Gy IR, and 1 h of recovery. Cells with more than 10 RAD51 foci were considered positive. Data are presented as mean ± SD. (H) Cell cycle analysis using propidium iodide (PI) staining in XRCC3 depleted U2OS cells expressing shRNA resistant HA-tagged WT/S225A XRCC3. Student's t-test, *$p < 0.05$; **$p < 0.01$; ***$p < 0.001$. n.s., non-significant.

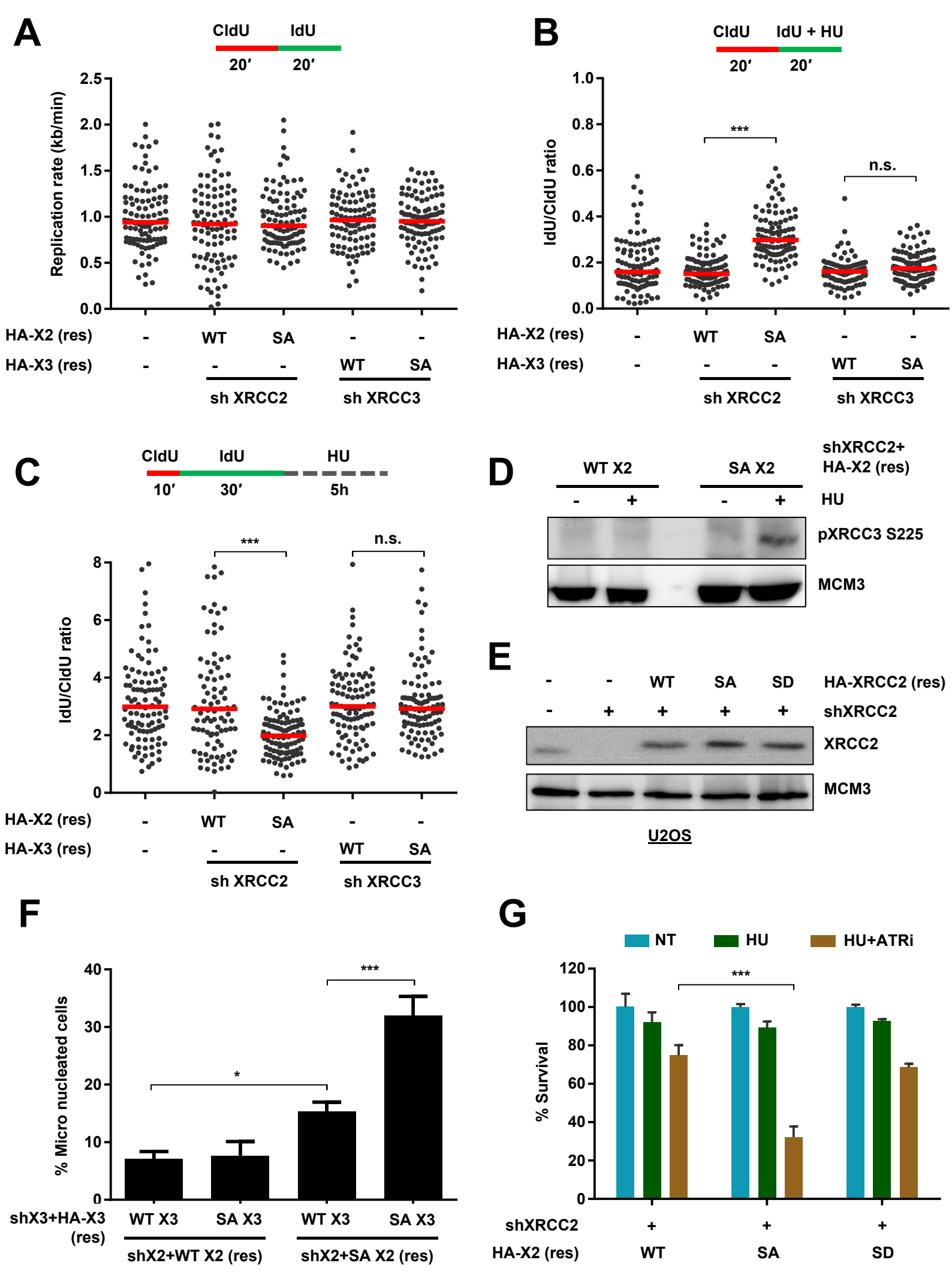
A
CldU
IdU
20′
20′
Replication rate (kb/min)
2.5
2.0
1.5
1.0
0.5
0.0
HA-X2 (res)
HA-X3 (res)
WT
SA
sh XRCC2
sh XRCC3
B
CldU
IdU + HU
20′
20′
IdU/CldU ratio
1.0
0.8
0.6
0.4
0.2
0.0
***
n.s.
C
CldU
IdU
HU
10′
30′
5h
8
6
4
2
0
D
shXRCC2+
HA-X2 (res)
WT X2
SA X2
HU
pXRCC3 S225
MCM3
E
HA-XRCC2 (res)
shXRCC2
XRCC2
MCM3
U2OS
F
% Micro nucleated cells
40
30
20
10
0
*
shX3+HA-X3
(res)
WT X3
SA X3
shX2+WT X2 (res)
shX2+SA X2 (res)
G
NT
HU
HU+ATRi
% Survival
120
100
80
60
40
20
0
shXRCC2
HA-X2 (res)
SD

Figure S4

Figure S4. Cells defective in XRCC2 phosphorylation undergo early XRCC3 S225 activation to promote cell survival. Related to Figures 3 and 4. (A) Replication rate in indicated U2OS cells. Each dot represents one fiber. A minimum of 100 DNA fibers were analyzed for each condition. HA-X2 (res), shRNA resistant HA-tagged XRCC2. (B) Quantification of IdU to CldU tract length ratios in indicated U2OS cells to study fork slowdown in the presence of HU (500 μM). (C) Quantification of IdU to CldU tract length ratios in indicated U2OS cells to study fork degradation following HU treatment (4 mM). (D) Analysis of XRCC3 S225 phosphorylation in indicated U2OS cells treated with 2 mM HU for 2 h. (E) Western blot showing expression of HA-tagged, shRNA resistant WT, S247A and S247D XRCC2 variants in XRCC2 depleted U2OS cells at levels comparable to endogenous levels. (F) Quantification of micronuclei in indicated U2OS cells after treatment with HU (150 μM) for 24 h. Data are presented as mean ± SD. (G) Survival of indicated U2OS cells upon exposure to 2 mM HU for 4 h, with or without continuous treatment of 1 μM ATRi (VE-821). Data are representative of 3 independent experiments. Data are presented as mean ± SD. DNA fiber labeling protocol is shown for individual panels. A minimum of 100 DNA fibers were analyzed for each condition. Student's t-test, *$p < 0.05$; **$p < 0.01$; ***$p < 0.001$. n.s., non-significant.

Table S1. Sequence of primers for generation of XRCC2 and XRCC3 constructs. Related to STAR Methods

PRIMER NAME	SEQUENCE (5′ - 3′)
XRCC2 Forward	ATAGAGGATCCATGTGTAGTGCCTTCCAT
XRCC2 Reverse (HA-his tag)	ATAGAGAATTCTCAGTGATGGTGGTGATGGTGTGCATAGTCGGGGACGTC ATAGGGGTAACAAAATTCAACCCCACT
XRCC2 (shX2#1 resistant) Forward	GACTATCGCCTGGTTCTTTTCGCGACCACGCAGACCATCATGCAGAAAGCC TCGAGCTCA
XRCC2 (shX2#1 resistant) Reverse	TGAGCTCGAGGCTTTCTGCATGATGGTCTGCGTGGTCGCGAAAAGAACCAG GCGATAGTC
XRCC2 S247A Forward	AAACAAGATGATGCACAAAGCAGCAAC
XRCC2 S247A Reverse	GTTGCTGCTTTGTGCATCATCTTGTTT
XRCC2 S247D Forward	AAACAAGATGATGACCAAAGCAGCAAC
XRCC2 S247D Reverse	GTTGCTGCTTTGGTCATCATCTTGTTT
XRCC3 (shX3#1 resistant) Forward	ATAGAGGATCCATGGATTTGGATCTACTGGACCTGAATCCCAGGATCATCG CCGCGATCAAAAAAGCCAAACTGAAATCG
XRCC3 Reverse (HA-his tag)	ATAGAGAATTCTCAGTGATGGTGGTGATGGTGTGCATAGTCGGGGACGTC ATAGGGGTAGTGGGACTGGGTCCCAGG
XRCC3 S225A Forward	TGTGAATTTGACGCCCAGGCCTCCGCC
XRCC3 S225A Reverse	GGCGGAGGCCTGGGCGTCAAATTCACA